Supporting information

Symmetry of the underlying lattice in (K,Na)NbO_3-Based Relaxor Ferroelectrics with large electromechanical response

Nan Zhang[1], Ting Zheng[1,*], Ning Li[3], Chunlin Zhao[1], Jie Yin[1], Yang Zhang[4], Haijun Wu[2,3,*], Stephen J. Pennycook[3], and Jiagang Wu[1,*]

[1]*Department of Materials Science, Sichuan University, Chengdu, 610065, P. R. China*

[2]*State Key Laboratory for Mechanical Behavior of Materials, Xi'an Jiaotong University, Xi'an 710049, China*

[3]*Department of Materials Science and Engineering, National University of Singapore, Singapore 117575, Singapore*

[4] *Instrumental Analysis Center of Xi'an Jiaotong University, Xi'an Jiaotong University, Xi'an 710049, China*

***Corresponding author:** wu.haijun@u.nus.edu (W. H. J); zhengtingscu@126.com (Z. T); wujiagang0208@163.com or msewujg@scu.edu.cn (W. J. G)

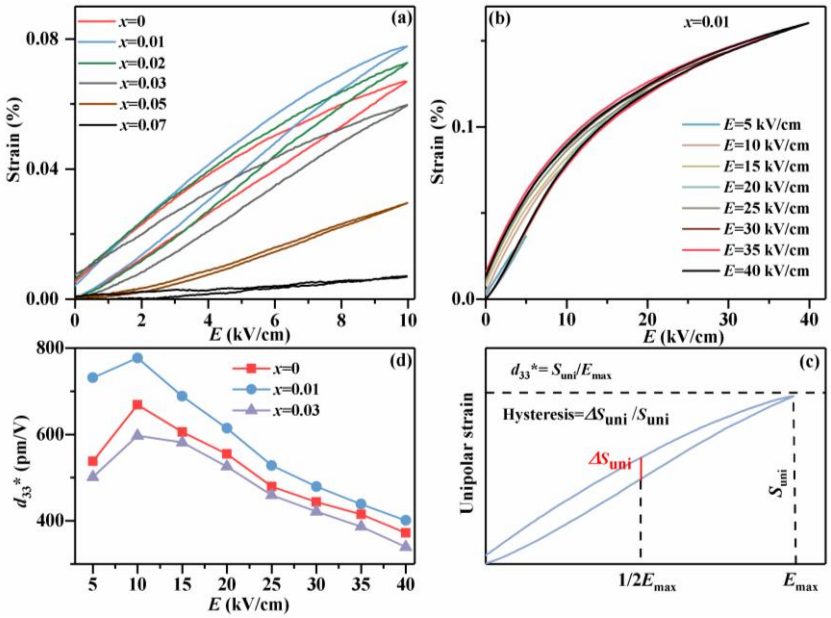

Figure S1. (a) Unipolar strain of $KNN_{1-x}S_x$-BNZ-AS-Fe ceramics with x=0-0.07 measured at E=10 kV/cm and f=5 Hz; (b) Unipolar strain of the ceramics with x=0.01 measured at different electric fields; (c) schematic illustrations for the strain hysteresis (hysteresis=$\Delta S_{uni}/S_{uni}$) and d_{33}* value (d_{33}*= S_{uni}/E_{max}) in unipolar S-E curves; (d)d_{33}* measured at different electric fields for the ceramics with x=0, 0.01 and 0.03.

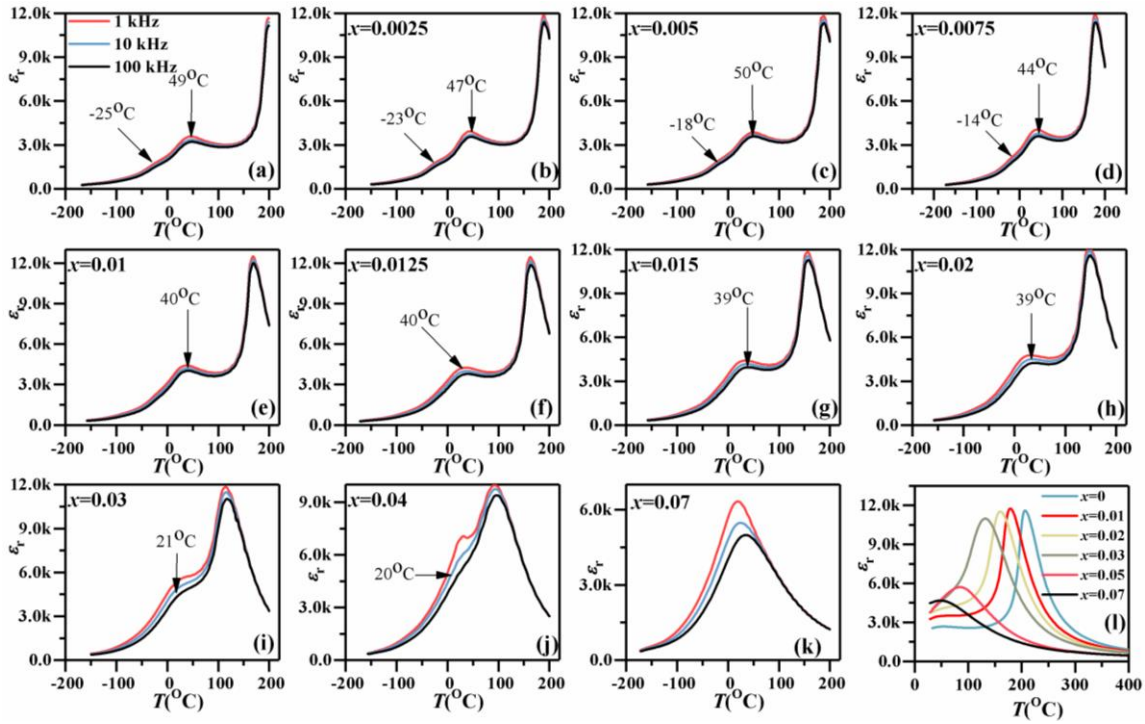

Figure S2 ε_r-T curves of $KNN_{1-x}S_x$-BNZ-AS-Fe ceramics with (a)-(k) x=0-0.07, measured at different frequency and -150-200 °C; (l) ε_r-T curves of $KNN_{1-x}S_x$-BNZ-AS-Fe ceramics, measured at 100 kHz and 25-500 °C.

Figures S2 (a-k) show the ε_r-T curves of the ceramics measured at -150-200 °C. Two/Three anomalous dielectric peaks can be observed in the ceramics with x=0-0.04, which represent rhombohedral-orthorhombic phase transition (*R*-*O*) and orthorhombic-tetragonal phase transition (*O*-*T*) and tetragonal-cubic phase transition (*T*-*C*).[1, 2] $T_{R\text{-}O}$ and $T_{O\text{-}T}$ of the ceramics with x=0-0.0075 are nearly to the room temperature. Thus, the phase structures of the ceramics with x=0-0.0075 are considered as the coexistence of *R*-*O*-*T*.[3] Moreover, the peaks of $T_{R\text{-}O}$ and $T_{O\text{-}T}$ became more successive or merge into one peak as x increased, confirming that the optimum addition of Sb can simultaneously increase $T_{R\text{-}O}$ and decrease $T_{O\text{-}T}$.[4, 5] With the further increase of x (x=0.05, 0.07), only one anomalous dielectric peak can be observed, which presents the *T*-*C* phase transition. Figure S2(l) shows the ε_r-T curves of the ceramics measured at 100 kHz and 25-500 °C. It can be seen that T_C gradually changes toward a low temperature, and becomes diffused at high x content. To further investigate the phase evolution of the ceramics, XRD patterns are given in Figure S3 (a) and (b). All ceramics present a pure perovskite structure, and no secondary phase can be observed, indicating that a stable solid solution is formed in the complicated doped KNN-based ceramics.[4, 6] As shown in Figures S2 and S3, *R*-*O* and *O*-*T* phase boundary can be observed in the ceramics with $0 \leqslant x \leqslant 0.0075$, leading to the

coexisting *R-O-T* phase in those ceramics. With the further increase of Sb content, an *R-O-T* phase boundary is observed in the ceramics with $0.01 \leqslant x \leqslant 0.02$. The ceramics with $0.03 \leqslant x \leqslant 0.04$ present suppressed *R-O-T* phase structure. Finally, a Pseudo-Cubic phase is observed in the ceramics with $0.05 \leqslant x \leqslant 0.07$. Figures S3 (c-h) show the rietveld refinement results of x=0, 0.01, 0.03, 0.04 and 0.07, respectively. The detailed refinement results are listed in Table S1. The refinement results of x=0, 0.01, 0.03, 0.04 are well consistent with the XRD results we discussed above. For x=0.07 ceramic, a combination of *P4mm* and *Pm3m* as well as pure *Pm3m* are used for Rietveld refinement, respectively, as shown in Figures S3 (g-h). The refinement using the combination of *P4mm* and *Pm3m* exhibits a better matching to the original data, which is demonstrated the lowest R_{wp} and *Sig* values, as listed in Table S1. Thus, the parameters of Pseudo-Cubic phase structure of the x=0.07 ceramic is similar to those of the coexistence of *P4mm* and *Pm3m* rather than pure cubic phase, where *P4mm* give the dominated contribution.

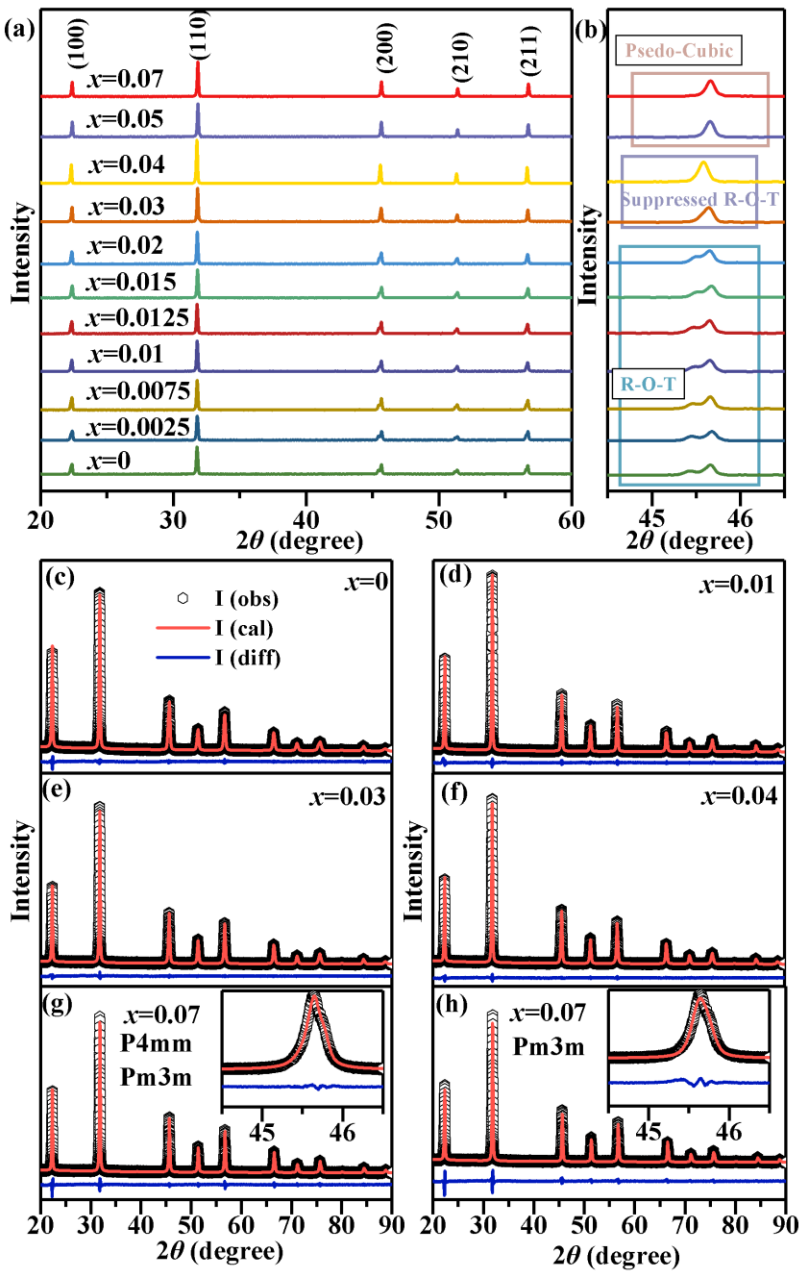

Figure S3 (a) XRD patterns of the ceramics; (b) Expand XRD patterns of the ceramics; (c-h) Rietveld refinement of XRD results for ceramics with x=0, 0.01, 0.03, 0.04 and 0.07.

Figure S4 shows the surface SEM images of the ceramics, and the corresponding grain size distribution is estimated by analytical software as shown in the inset of Figure S4. A bimodal grain size distribution could be found in the all measured

ceramics, which has been widely reported in other KNN-based ceramics.[7, 8]

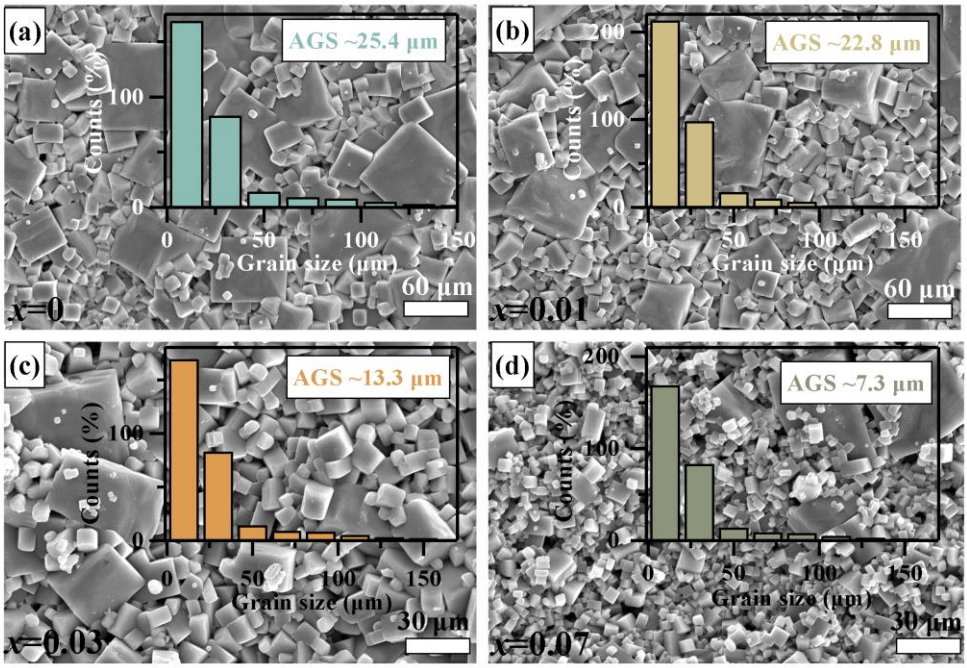

Figure S4 SEM surface images of ceramics with (a-b) *x*=0, 0.01, 0.03 and 0.07, the inset is the corresponding grain size distribution and average grain size (AGS).

The low roughness in topography (<5 nm) indicates the good polishing process (Figures S5a, c and S6a1, b1, c1). Besides, the topographies show some remarkable scratches, which is beneficial to differentiate domains and topography. In addition, all the PFM amplitude and phase images show no similar patterns to those of the topography, illustrating the true detection (Figures S5 and S6). In addition, although nano-sized domains could be observed in the ceramics with *x*=0, 0.01 and 0.07, distinct difference could be found among these three compositions (Figure S6). Decreased sized and increased amount of nanodomains could be observed in the ceramic with *x*=0.01 compared to *x*=0 (Figures S6a1-b3), demonstrating that the appropriate addition of Sb could significantly reduce the size of domains and increase

the fraction of nanodomains. With the further increasing *x* content to *x*=0.07, the long range ordered ferroelectric domain almost be broken up thoroughly, and only a few nanodomains is observed (Figures S6c1-c3). In this case, the high content doping composition (*x*=0.07) could be regarded as relaxor, which is almost entirely composed of polar nanoregions.[9]

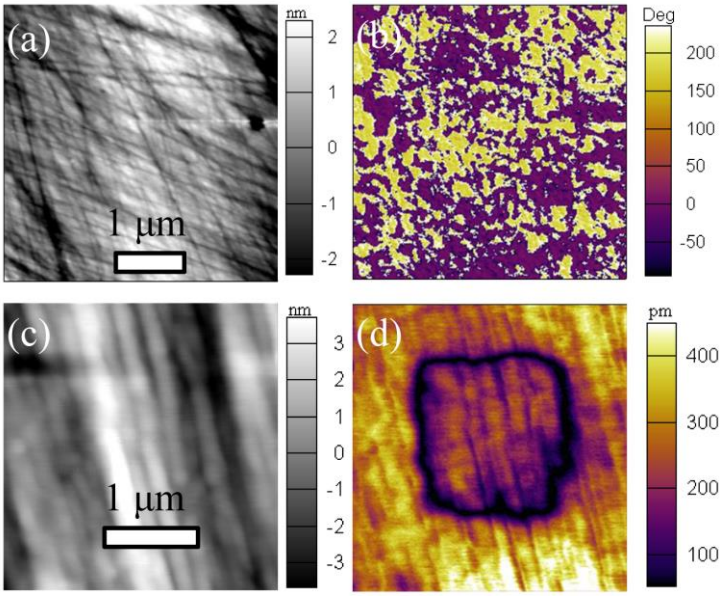

Figure S5 (a) Topography and (b) phase images of the V-PFM for the ceramics with *x*=0.01; (c) Topography and (d) amplitude images PFM after poling with ±8 V voltage of *x*=0.01 ceramic.

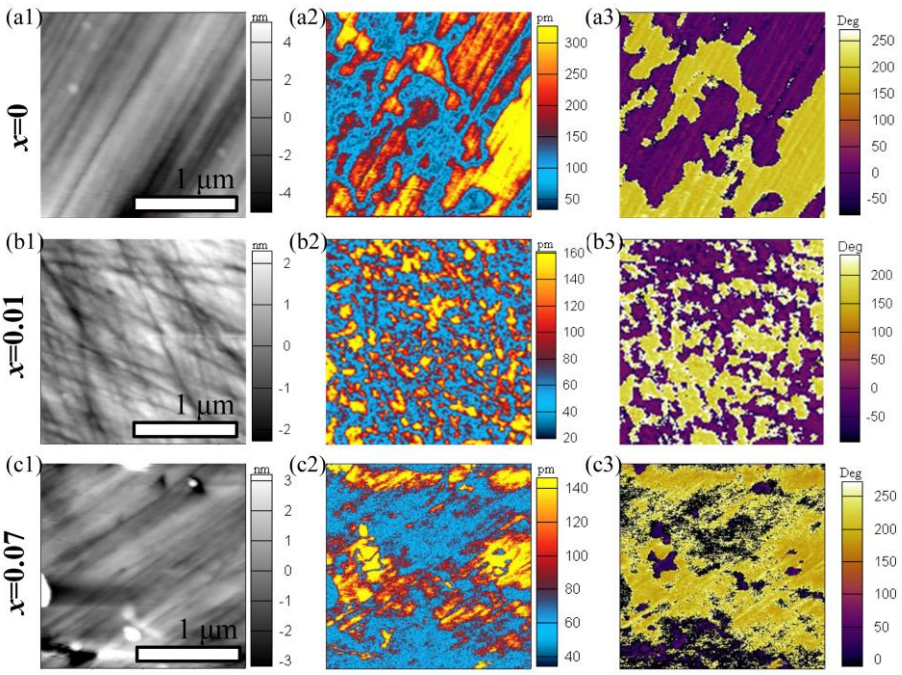

Figure S6 V-PFM topography, amplitude and phase images of (a1-a3) x=0, (b1-b3) x=0.01, (c1-c3) x=0.07.

Figures S7 (a-d) show the $\ln(1/\varepsilon_r-1/\varepsilon_m)$ versus $\ln(T-T_m)$ images of the ceramics, and the slope of the fitting is the value of γ. Modified Curie-Weiss law can be used to evaluate the diffuseness degree (γ) of the ceramics: $1/\varepsilon_T-1/\varepsilon_m=(T-T_m)^\gamma/C$, where ε_m is the maximum permittivity at T_m and C is the Curie-like constant.[10, 11] It is well known that γ=1 represents a classical ferroelectric, while γ=2 represents a typical relaxor and $1<\gamma<2$ represents a relaxor ferroelectric.[12]

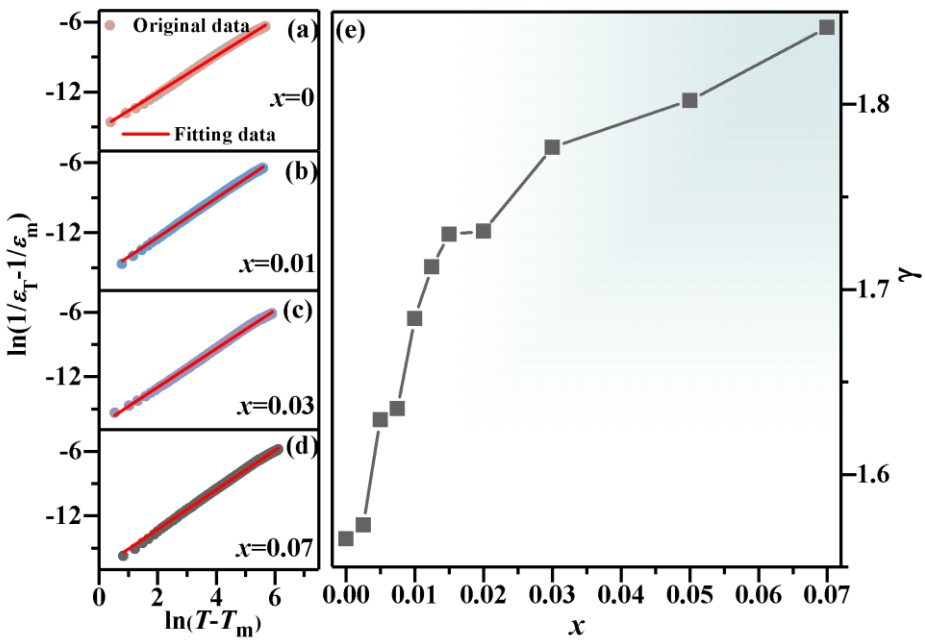

Figure S7 (a-d) ln(1/ε_r-1/ε_m) versus ln(T-T_m) images of the ceramics; (e) Composition dependence of the calculated degree of diffuseness γ.

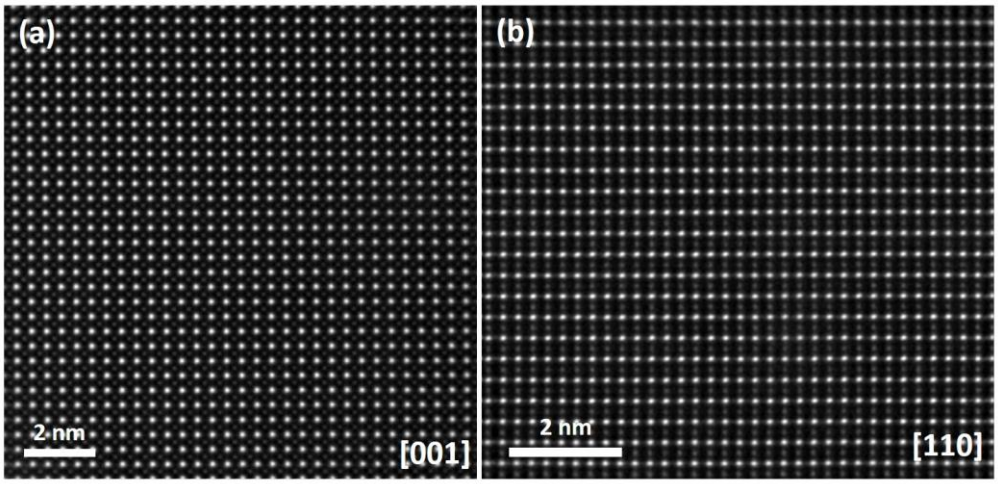

Figure S8. Atomically-resolved STEM HAADF image along (a) [001] and (b) [110] zone axes, which are simultaneously acquired with the STEM ABF images in Figure 4(a, d) respectively.

Table S1 Structure parameters of the ceramics with x=0, 0.01, 0.03 and 0.04.

Composition	*Sig*	R_w (%)	Space group (%)	a (Å)	b (Å)	c (Å)	α (°)
			R3m (38.86)	3.9834	3.9834	3.9834	89.9871
x=0	1.43	3.11	Amm2 (33.91)	3.9626	5.6034	5.6715	90
			P4mm (27.23)	3.9673	3.9673	3.9850	90
			R3m (38.75)	3.9873	3.9873	3.9873	89.6291
x=0.01	1.64	3.88	Amm2 (38.87)	3.9716	5.6044	5.6782	90
			P4mm (22.38)	3.9712	3.9712	3.9861	90
			R3m (39.96)	3.9772	3.9772	3.9772	89.9505
x=0.03	1.52	3.48	Amm2 (35.76)	3.9720	5.6052	5.6640	90
			P4mm (24.28)	3.9705	3.9705	3.9822	90
			R3m (45.96)	3.9764	3.9764	3.9764	89.9707
x=0.04	1.35	3.07	Amm2 (29.72)	3.9737	5.6084	5.6671	90
			P4mm (24.32)	3.9703	3.9703	3.9802	90
			P4mm (91.90)	3.9711	3.9711	3.9798	90
x=0.07	1.87	4.31					
			Pm3m (8.10)	3.9698	3.9698	3.9698	90
x=0.07	2.40	5.51	Pm3m (100)	3.9713	3.9713	3.9713	90

References

(1) Tao, H.; Wu, H.; Liu, Y.; Zhang, Y.; Wu, J.; Li, F.; Lyu, X.; Zhao, C.; Xiao, D.; Zhu, J.; Pennycook, S. J. Ultrahigh Performance in Lead-Free Piezoceramics Utilizing a Relaxor Slush Polar State with Multiphase Coexistence. *J. Am. Chem. Soc.* **2019**,

141, 13987-13994.

(2) Lv, X.; Wu, J. Effects of a Phase Engineering Strategy on the Strain Properties in KNN-Based Ceramics. *J. Mater. Chem. C* **2019**, *7*, 2037-2048.

(3) Zhou, C.; Zhang, J.; Yao, W.; Liu, D.; He, G. Remarkably Strong Piezoelectricity, Rhombohedral-Orthorhombic-Tetragonal Phase Coexistence and Domain Structure of (K,Na)(Nb,Sb)O_3–(Bi,Na)ZrO_3-$BaZrO_3$ Ceramics. *J. Alloy. Componds.* **2020**, *820*, 153411.

(4) Wang, X.; Wu, J.; Xiao, D.; Zhu, J.; Cheng, X.; Zheng, T.; Zhang, B.; Lou, X.; Wang, X. Giant Piezoelectricity in Potassium-Sodium Niobate Lead-Free Ceramics. *J. Am. Chem. Soc.* **2014**, *136*, 2905-2910.

(5) Wu, J.; Xiao, D.; Zhu, J. Potassium-Sodium Niobate Lead-Free Piezoelectric Materials: Past, Present, and Future of Phase Boundaries. *Chem. Rev.* **2015**, *115*, 2559-2595.

(6) Li, J. F.; Wang, K.; Zhu, F. Y.; Cheng, L. Q.; Yao, F. Z.; Green, D. J. (K,Na)NbO_3-Based Lead-Free Piezoceramics: Fundamental Aspects, Processing Technologies, and Remaining Challenges. *J Am Ceram Soc.* **2013**, *96*, 3677-3696.

(7) Lv, X.; Wu, J.; Zhang, X. X. A New Concept to Enhance Piezoelectricity and Temperature Stability in KNN Ceramics. *Chem. Eng. J.* **2020**, *402*, 126215.

(8) Wu, B.; Ma, J.; Wu, W.; Chen, M. Improved Piezoelectricity in Ternary Potassium-Sodium Niobate Lead-Free Ceramics with Large Strain. *J. Mater. Chem. C* **2020**, *8*, 2838-2846.

(9) Huang, Y.; Zhao, C.; Wu, B.; Wu, J. Multifunctional $BaTiO_3$-Based Relaxor

Ferroelectrics toward Excellent Energy Storage Performance and Electrostrictive Strain Benefiting from Crossover Region. *ACS Appl. Mater. Interfaces* **2020**, 12, 23885-23895.

(10) Liu, Q.; Zhang, Y.; Gao, J.; Zhou, Z.; Wang, H.; Wang, K.; Zhang, X.; Li, L.; Li, J. F. High-Performance Lead-Free Piezoelectrics with Local Structural Heterogeneity. *Energ. Environ. Sci.* **2018**, *11*, 3531-3539.

(11) Ding, Y.; Zheng, T.; Zhao, C.; Wu, J. Structure and Domain Wall Dynamics in Lead-Free KNN-Based Ceramics. *J. Appl. Phys.* **2019**, *126*, 124101.

(12) Zhao, C.; Yang, J.; Huang, Y.; Hao, X.; Wu, J. Broad-Temperature-Span and Large Electrocaloric Effect in Lead-Free Ceramics Utilizing Successive and Metastable Phase Transitions. *J. Mater. Chem. A* **2019**, *7*, 25526.